Experimental and Simulation Studies of Dust Transport in JT-60U Tokamak

N. Asakura[1], T. Hatae[1], Y. Tanaka[2], T. Hayashi[1], N. Ashikawa[3], A.Yu.Pigarov[4], H. Takenaga[1], T. Nakano[1], Y. Uesugi[2], N. Ohno[5]

1) Japan Atomic Energy Agency, Naka, Ibaraki 311-0193 Japan
2) Electrical Engineering and Computer Science, Kanazawa Univ., Kanazawa 920-1192 Japan
3) National Institute for Fusion Science, Toki, Gifu 509-5292 Japan
4) University of California at San Diego, La Jolla, California 92093 USA
5) Graduate School of Engineering, Nagoya Univ., Nagoya 464-8603 Japan

E-mail: asakura.nobuyuki@jaea.go.jp

ABSTRACT: Dust research has been performed in JT-60U in order to predict the plasma performance and the tritium retention in a fusion reactor. Laser scattering measurement showed that numbers of carbon dust were ejected in the main chamber at disruptions and in the following discharges. Radial distribution in the main vacuum chamber at the disruption was relatively uniform, suggesting that they were redistributed over the wide surface area. In the following discharge, both the size and number were peaked in the far-SOL and they decreased near the separatrix. This result shows that sublimation of dust is dominant in the SOL. Lifetime until the sublimation and the distance from the separatrix were calculated to be 2 - 200 ms and 22 - 4 cm with increasing the dust radius of 0.1-100 mm, respectively. Experimental and simulation results showed very few probability of the penetration into the confined plasma as an impurity source. Dust collection after the experiment campaign showed that large weight of the dust was cumulated on the exhaust route of gas flow under the divertor. Microscope analysis showed the main population of small dust (less than 20 μm) had a statistical distribution, and number of large dust (larger than 20 μm) contributed significantly to the total weight. On the other hand, both are necessary to evaluate the cumulative surface area for determination of the tritium retention.

1. Introduction

Understanding of the dust transport as well as determination of where it is ejected and finally deposited are necessary to predict the plasma performance and the tritium retention in a fusion reactor. Experimental studies of the dust movement and distribution in the plasma are required to investigate its influence on the impurity concentration in the main plasma. Determination of the dust deposition on the plasma-exposed surface and the shadow area, i.e. behind the plasma facing components (PFCs), is required in order to evaluate an important potential source of the tritium retention. Development of the dust transport model will explain the process from the dust ejection to its sublimation or deposition in the vacuum vessel.

Experimental results of the dust transport and distribution in the plasma discharges have been recently reported in tokamaks and stellarator [1-3]. In the JT-60U tokamak, experimental and modelling studies have been developed to understand transport and deposition processes of carbon dust [4]. Nd-YAG laser Thomson scattering system [5] was applied for the detection of dust scattering light ("Mie scattering"): distributions of the scattering signals and their intensity were determined. At the same time, visible images emitted during its ablation in the main plasma and divertor were measured with a fast TV camera. The transport simulation of the ablating dust in the SOL plasma has been developed using DUSTT code [6]: the lifetime until the sublimation and the distance from the separatrix were calculated for various size of dust. Dust collection in the vacuum vessel such as the divertor (including the plasma-exposed surface and the shadow area), baffle and first wall, was performed after the final experiment campaign of 2008. Analysis result of the area density is presented.

2. Dust Distributions at Disruption and in Plasma Discharges

Distribution of the Laser scattering signal above the outer baffle was measured, as

shown in Fig. 1, with the pulse repetition of 50 Hz. Dust scattering signals in plasma discharges including the startup and termination were investigated. Telescope of the fast digital TV camera system was installed at a horizontal port, viewing the plasma discharge tangentially. Dust movement in the main chamber and divertor was measured by installing the wide- and narrow-view telescopes, respectively. Viewing area for the wide-view telescope and camera setting with 512x512 pixel/frame (6 kHz) is shown in Fig. 1.

Numbers of dust scattering signals were observed in some specific discharges. During and after the plasma quench at the disruption (t = 9.25 s), many dusts were observed in all locations as shown in Fig. 2(d). Here, the disruption was produced by injection of high-Z (Kr) gas in an ohmic heating plasma as a series of the impurity transport experiment. Each pulse signal ("event") and the intensity correspond to the scattering signal by a dust particle and its relative size (assuming a spherical shape), respectively [1]. Both event number and its intensity increase during and just after the plasma termination (t = 9.2 - 9.5 s) when the main plasma radiation power and the neutral pressure reach the maximum values (P_{rad}^{main} = 13 MW, p_0^{main} = 0.3 Pa). High event frequency and large intensity are seen when the high p_0^{div} and p_0^{main} are maintained (t = 9.5 - 10 s). Then, they decrease with decreasing p_0^{div} and p_0^{main} (t = 10 - 12 s).

Distributions of event frequency during three periods and t = 12 - 14 s are shown in Fig. 3. The separatrix location is 4 cm below the case in Fig. 1. It was found that numbers of dust are ejected into the main chamber during the plasma termination, and they spread over all main chamber when the high neutral pressure changes. This fact suggests that dust is redistributed over a wide surface area when the disruption occurs.

In the high power ELMy H-mode discharges (I_p = 1.6 MA, P_{NBI} = 16 MW and Fig. 1 shows the plasma configuration) just after another disruption,
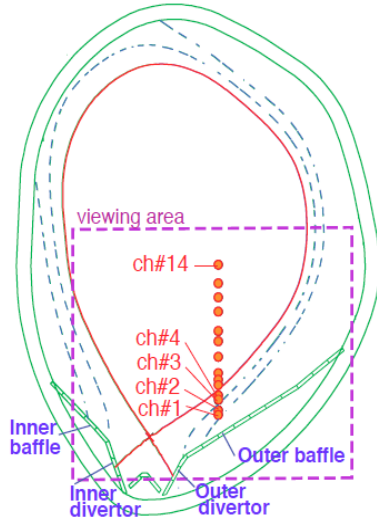

Fig.1 Plasma configuration of shot 49530, 14 locations of YAG laser scattering channels (closed circles), and viewing area of fast TV camera with 512x512 pixel and wide-view telescope (square frame).
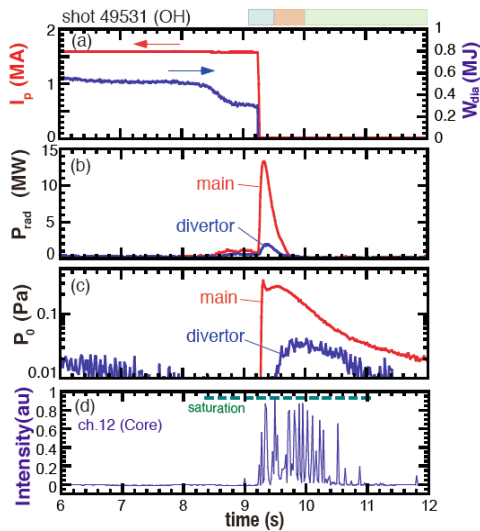

Fig.2 Time evolution of (a) plasma current, stored energy, (b) radiation losses in the main and divertor, (c) deuterium pressures in main chamber and sub-divertor, and (d) scattering signal in channel 12.
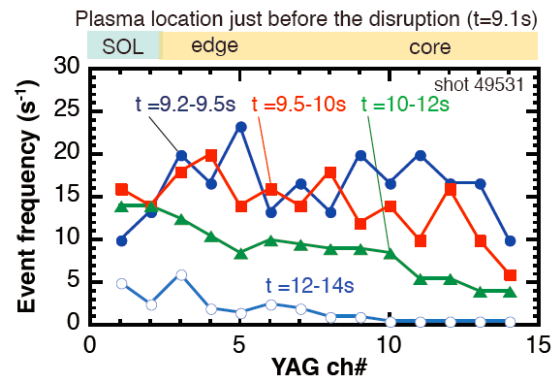

Fig.3 Radial profile of scattering event frequency during and after the disruption.

many and large dusts were ejected, as shown in Fig. 4, compared to discharges after the normal termination. It was often observed when the inner strike-point was higher than the normal operation, i.e. staying at thick deposition layers on the upper divertor tiles [7, 8].

Figure 5 shows a fast TV camera image of visible light emission from numbers of dust ejected from the surface of the divertor and outer baffle tiles, which can be traced within 1 ms. Numbers of dust are seen at the peripheral channels just above the outer baffle, where distance of ch.1 and ch.2 from the separatrix is 14 - 18 cm. Figure 4 shows that event number increases even during the low power L-mode (P_{NB} = 2 - 6 MW), then the event number decreases during the ELMy H-mode (P_{NB} = 15 MW). Increments of the SOL plasma density and SOL decay length during the L-mode may enhance the plasma interaction to the PFC surface. This result suggests that dust deposited on the plasma-exposed surface at a disruption is sublimated or transported into the shadow area such as between titles and below the divertor exhaust slot.

Figure 6 shows distributions of the event frequency (f^{dust}) and average intensity (I^{dust}) during 3 s after NBI start. For the cases just after disruption (shots 49530 and 49533), both f^{dust} and I^{dust} in the far-SOL (ch.1 and ch.2) are significantly large compared to those in the discharge after the normal termination (49537). Figure 7 shows distributions of event frequency averaged over adjacent 2 to 4 channels at the far-SOL and near-SOL (12 - 16 cm and 1 - 5 cm
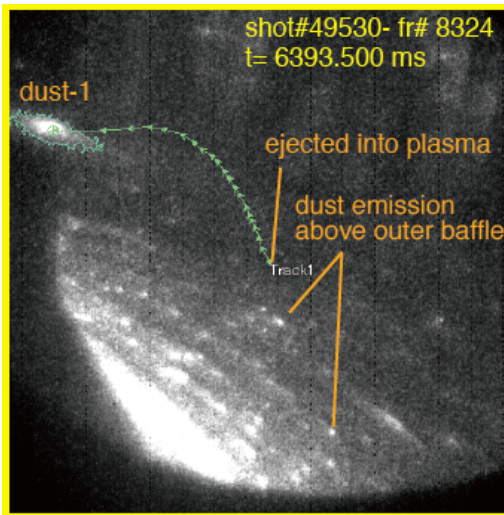

Fig. 4 Time evolution of (a) I_p, P_{NBI}, (b) electron density and recycling flux in the divertor for the ELMy H-mode plasma just after disruption. (c-e) Laser scattering signals in the SOL (ch.1, 2 and 4) are presented.

Fig.5 Visible light emission image from numbers of dust above the outer divertor and baffle at t = 6.3935 s. One dust (dust-1) moves from the outer baffle to the upper (poloidally) and forward (toroidally) direction during 7.5 ms.
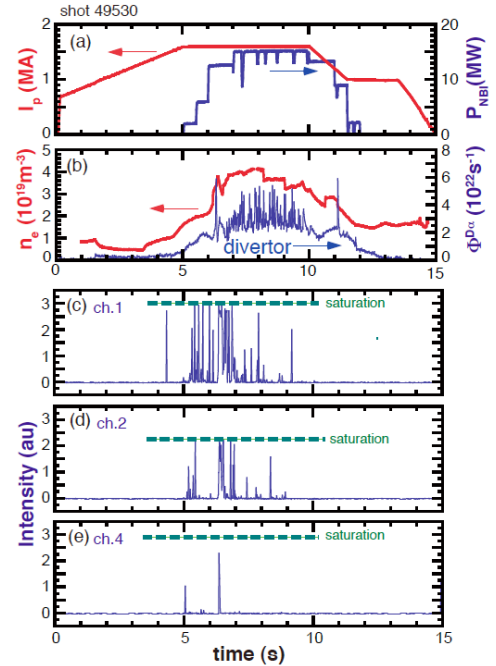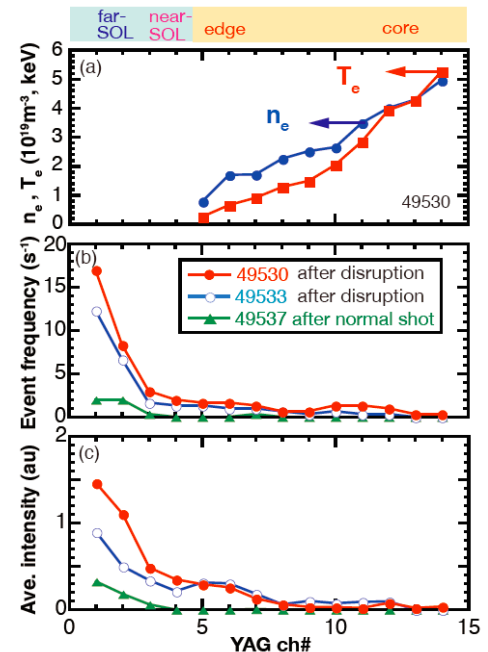

Fig.6 Profiles of (a) typical electron temperature and density in ELMy H-mode plasma, (b) event frequency, (c) average intensity during 3s after NBI start, for just after disruptions and following normal discharge.

3

outside the separatrix, respectively), and the edge and core plasmas (4 - 8 cm and 70 - 80 cm inside the separatrix, respectively): both the event frequency and the dust size decrease near the separatrix (providing signal intensity proportional to r^a, where r is the dust radius and $a = 2$), suggesting that sublimation of dust is dominant even in the SOL. Assuming the dust influx into the far-SOL is proportional to $f^{dust} \cdot r^3$, only 2.4 % and 0.3 % of the total carbon dust at the far-SOL are penetrated into the edge and core plasmas, respectively.

Fig.7 Distributions of event frequency as a function of signal intensity for the different positions: event data was obtained in three discharges just after

3. Dust Ejection and Movement in Divertor:

Dust movement was measured with the fast TV camera as a bright spot image of line emission from the carbon and hydrogen ions. Generally speaking, appearances of the dust emission as well as the scattering signal were very few in the routine operations even for high power NB injection. On the other hand, ejection of carbon dust from the inner divertor plate was often observed just after ELM event when the strike-point at the inner divertor was higher than the normal operation, i.e. on the soft deposition layers. Figure 8(b) shows tracking trajectories of two relatively large dusts (dust-2 and dust-3): the former is sublimated at t = 4.65 ms and the latter moves outside the viewing area. All dust particles move poloidally outwards and toroidlly in the plasma current direction. Velocities of dust-2 and dust-3 (V^{dust}) are evaluated to be 2.4 - 3.8 km/s and 1.7 - 3.2 km/s, respectively, assuming the toroidal movement. It is found that dust is accelerated 1.5 - 1.8 times after start of the emission (maybe during ablation). Lifetimes until the sublimation are plotted as a function of averaged V^{dust} in Fig. 9 (circles). Smaller dusts are also often ejected from the inner divertor after ELM events, and the lifetime (~1 ms) is shorter but slightly larger V^{dust} (0.2-0.35 km/s) compared to the large dusts (dust-2 and dust-3). The direction of the toroidal movement for all dusts is the plasma current direction, which is consistent with the SOL flow measuremed above the inner baffle [9]. Velocity ratio, V^{dust}/V^{plasma}, is 1-1.5%, and the acceleration may be caused by the friction force from the SOL plasma or asymmetry of the ablation along the field line [10].
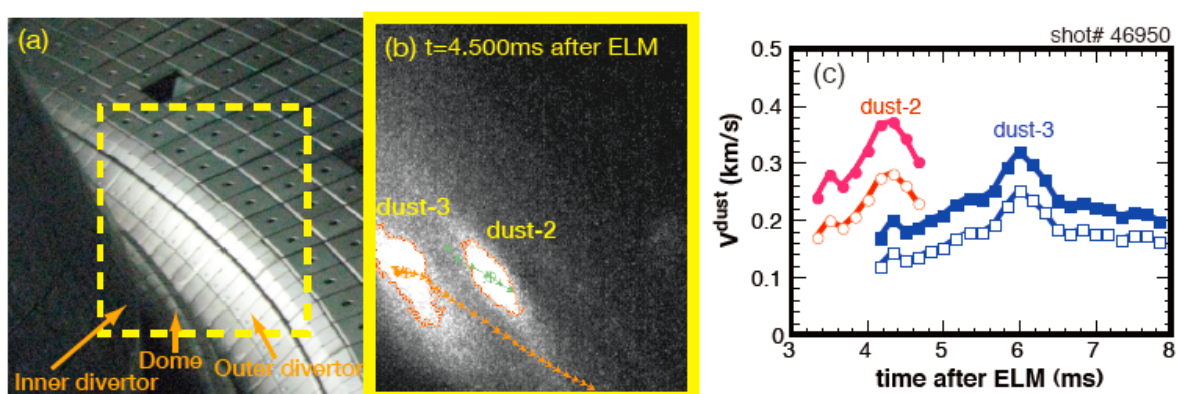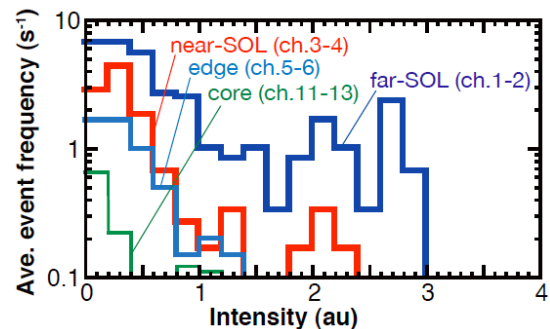

Fig.8 (a) Fast TV view in the divertor using narrow-view telescope. (b) dust emission image at t = 4.500 ms after an ELM event and tracking trajectories. (c) dust velocities in 2-d poloidal cross-section (open symbols) and 3-d movement in the toroidal direction (closed symbols).

Whereas lifetime of most dust is short (less than one ms) near the surface of the baffle plates, one of dusts ejected from the outer baffle plate can be tracked with a long lifetime (3.4

ms) as shown in Fig. 5: it appears above the outer baffle at P-12 section and is moving upwards against the gravity force and toroidally towards P-17 port (angle of 100°). The plasma toroidal rotation in the confined plasma changed from the co-direction in the edge (+15 km/s) to the counter-direction in the core (-70 km/s). The dust may pass though the edge of the confined plasma. Analysis of the dust image determined relatively fast V^{dust} of 0.2 - 0.35 km/s in the plasma current direction, which is comparable to those in the divertor.

Fig.9 Average dust velocities and lifetime in the main and divertor plasmas, including dust-1(Fig.5) and dust-2 and dust-3(Fig.8).

4. Simulation of Dust Penetration in SOL:

Carbon dust trajectories ejected from the different locations such as the divertor and baffle were calculated by DUSTT-code. Lifetime of dust until the sublimation and its penetration into the plasma were evaluated for the different radii of the spherical dust (r_d = 0.1, 1, 10, 100 μm) with the initial velocity of zero. Fig. 10 shows dust transport in the poloidal cross-section ejected from the outer baffle plate, and time evolutions of the temperature, radius and velocity [11]. Dust transport is influenced by the ion friction force in most area of the SOL, while electric field produced at the surface sheath affects it to remove from the surface.

Lifetime is increased from 2.2 to 195 ms with r_d increasing, and the distance from the separatrix at the sublimation decreases from 22 to 4 cm. The simulation results show that sublimation of dust is dominant even in the SOL, which is consistent with the laser scattering measurements. On the other hand, the maximum velocities near the sublimation (0.01-0.1 km/s) are smaller and the lifetimes are longer than the fast TV measurements. Further investigation of the ablating dust transport will be required in the modelling and measurement.

Fig.10 (a) Trajectories ejected from the outer baffle until sublimation (circles) for 0.1, 1, 10, 100 μm radii. Time evolutions of (b) temperature, (c) radius, and (d) velocity.

5. Carbon Dust Deposition in Divertor:

Carbon dust deposition in vacuum vessel was investigated [7,13] after 2002 experiment campaign of JT-60U, i.e. 6 years operation after installation of the W-shaped divertor. Dust collection at the divertor, baffle and first wall, was recently performed after the final experiment campaign of 2008, using numbers of collection holders with a sneezing nozzle and a membrane filter (the pore-size of 0.1 μm). Dust collection at the divertor and first wall surfaces in the different toroidal sections was performed, but the analysis was not completed. Here, analysis result of one poloidal section in the divertor is presented since most dust was cumulated on the lower vacuum vessel [7]. Plasma-exposed surface and shadow area in the divertor and baffle are divided by 14 and 6 poloidal regions, respectively, as shown in Fig. 11.
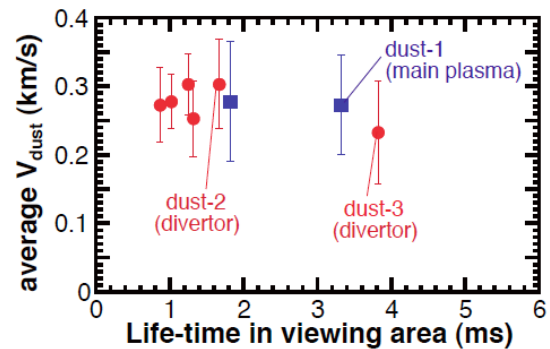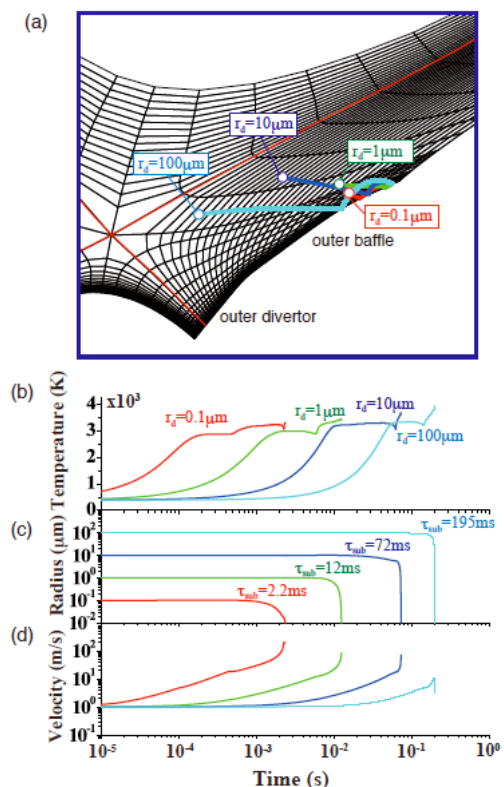
5.1 Distribution of Dust Weight Density

Figure 12 shows the distributions of area density of the dust weight at the plasma-exposed surface and shadow area. At the plasma-exposed surface, large area densities (w^{dust}) of 2.3 and 60 mg/m^2 are seen at the upper tiles of the inner divertor, comparing to w^{dust} = 0.32 mg/m^2 for the lower tile of the inner divertor, w^{dust} = 0.42 - 1.43 mg/m^2 for the dome and w_{dust} = 0.73 - 0.80 mg/m^2 for the outer divertor tiles. Relatively thick carbon deposition layers are seen on the surface of the upper inner divertor tiles [7,8], and the soft deposition would be relatively easy to be removed by the high temperature plasma flux as described in Sec. 3. Area densities on the inner and outer baffles (w^{dust} = 0.09 - 0.35 mg/m^2) are smaller than those in the divertor. On the other hand, area densities at the shadow area are generally large, in particular, under the dome (w^{dust} = 230 - 510 mg/m^2), which are comparable to or larger than those observed in 2003 [7]. Area density at the tile side was also measured: it is comparable to the surface w^{dust} for the inner divertor, while smaller than the surface w^{dust} for the other regions. Analysis under the inner and outer baffle plates will be done.

From these results, the total dust weight collected in the vacuum vessel is estimated assuming their toroidal symmetry. The total dust weights at the plasma-exposed surface and the shadow areas are 1.32 g and 22.23 g, respectively. Dust at the shadow area is 17 times larger than that at the plasma-exposed surface. Number of dust was cumulated under the divertor, i.e. on the exhaust route of the gas flow produced by the divertor pumping, which suggests large potential source of the hydrogen isotope retention.

5.2 Analysis of Dust Particle Population

Size and surface area of the dust particles affect the hydrogen isotope retention. Dust images on the membrane filter were taken into digital data by the digital microscope, and dust size and shape such as average diameter (*d*) were determined by an image analysis software. Number distribution of the average diameter is investigated. Spatial resolution for 700- and 3500-magnified microscope images correspond to 0.275 and 0.055 μm/pixel, which are mainly used for the relatively large and small dust database, respectively. Figure 13 shows two representative results of the dust image analysis for the deposition dominant regions, i.e.
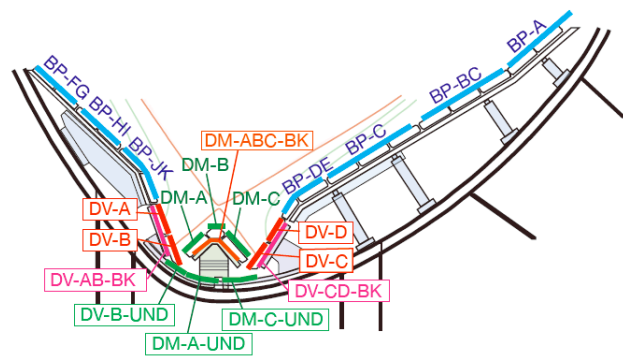

Fig.11 Dust collected regions in the divertor and baffle. DV-AB-BK, DV-CD-BK, DM-ABC-BK show surfaces of base plates at the inner divertor, outer divertor and dome, respectively (shadow area). DV-B-UND, DM-A-UND, DM-C-UND correspond to surfaces of cooling base under the inner divertor (including inner exhaust opening), and inner- and outer-side of the dome (including outer exhaust opening), respectively.
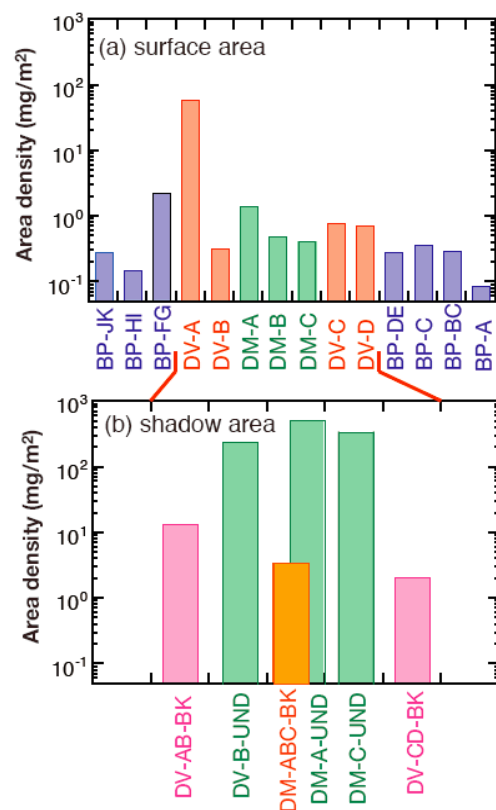

Fig.12 Distributions of area density of dust weight at (a) plasma-exposed surfaces, and (b) shadow area.

the upper inner divertor (DV-A) and under the dome (DM-C-UND): number distribution and cumulative volume assuming spherical shape of the dust ($\pi/6 \cdot d^3$). Comparison between plasma-exposed surface and the shadow area shows that the average dust size of the main population is less than 20 μm, and the distribution of the shadow area becomes wider.

Large dusts (larger than 20 μm) are often observed at the deposition-dominant surface and the shadow area, and number of large dust contributes significantly to the total dust weight. Although number of the large dust in two examples is incidental, the total weight of large dust corresponds to 98.5% and 92% in Fig. 13 (a) and (b), respectively, assuming the same density for all dust. Large dust images were investigated by Scanning Electron Microscope (SEM). Most large dust consists of small peaces or flakes of the deposition layers as shown in Fig.14 (a), which are often found both at the inner target and under the dome, suggesting they are removed from the soft deposition layers. While cauliflower-like dust shown in Fig.14 (b) was also often found at both regions, the origin was not determined. Weight densities of the two kind dusts may be different.

Detail distribution of the average dust size in the main population (smaller than 20 μm) is investigated for the erosion-dominant tiles of the dome (DM-B) and deposition-dominant tiles (DV-A) as shown in Fig. 15. While probability distributions of the small dust (0.2 μm ≤ d ≤ 4 μm) are comparable, upper limit of the dust size for DM-B (5-6 μm) is smaller than

Fig.13 Number distribution of dust diameter and cumulative volume (a) at the upper inner divertor (DV-A) and (b) under the dome (DM-C-UND).
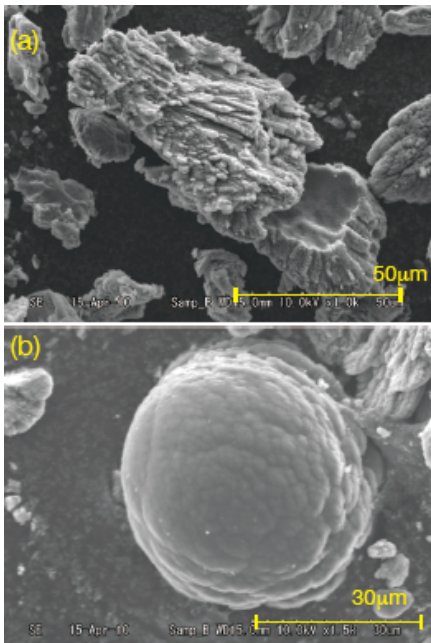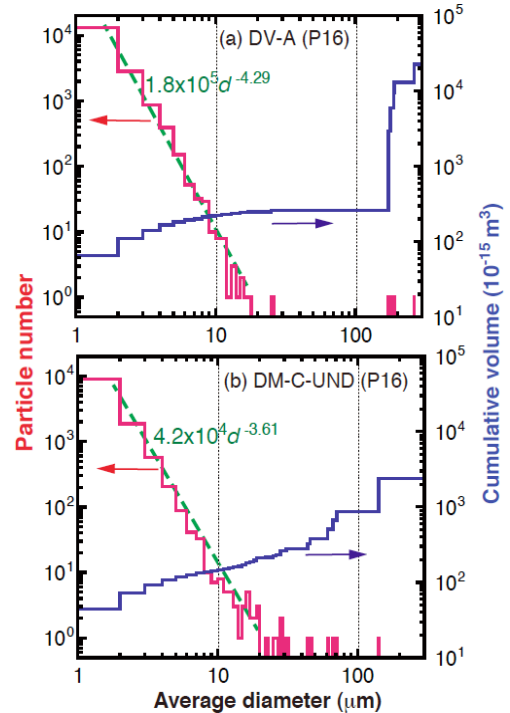

Fig.14 Representative SEM image of large dust collected at deposition-dominant tiles (DV-A).
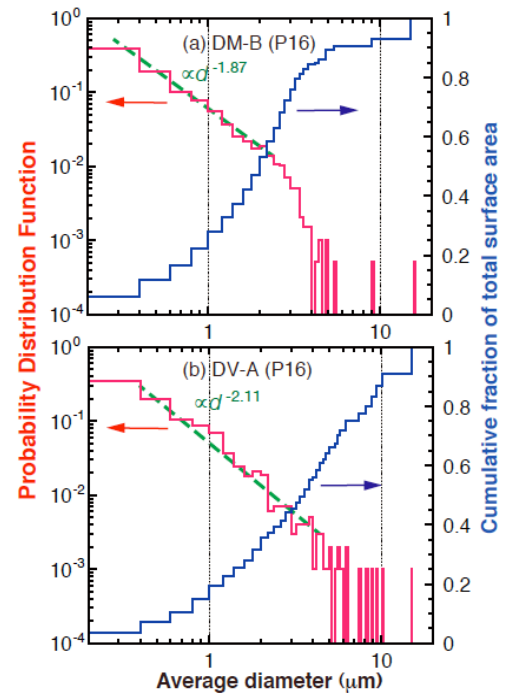

Fig.15 Probability distribution of dust diameter and cumulative surface area fraction at (a) the dome top (DM-B) and (b) the upper inner divertor (DV-A).

7

that for DV-A (~10 μm). Cumulative surface area fraction, assuming spherical shape of the dust ($\pi \cdot d^2$), shows that small dust ($d \leq 1$ μm) also contributes to the total surface area: 27% and 20% for DM-B and DV-A, respectively. Since our sampling method may be available for $d \geq 0.1$ μm, determination of very small dust number ($d \leq 0.1$ μm) will be important for accurate evaluation of the total surface area and the hydrogen isotope retention, especially for the erosion-dominant tiles. For the deposition-dominant region, the total cumulative surface area fraction of the main population (1 μm $\leq d \leq$ 20 μm) is 38% of the total surface area (1 μm $\leq d \leq$ 300 μm) in the large dust analysis. Thus, contribution of the very small dust on the total surface area would be less important.

6. Summary and Conclusion:

Systematical dust research has been developed in JT-60U tokamak. Laser scattering measurement showed that huge number of carbon dust was ejected in the main chamber at disruptions and in the following discharges. The radial distribution during and just after the plasma termination at the disruption was relatively uniform, suggesting their redistribution over the main chamber. In the following discharge, both the dust size and number were peaked in the far-SOL, thus the sublimation is dominant in the SOL. Fast TV measurement showed that carbon dust was often ejected from the soft deposition layers at the upper inner divertor tiles just after ELM event, and the fast movement towards the toroidal direction (0.3-0.4 km/s) was evaluated.

Lifetime until the sublimation and the distance from the separatrix were calculated, using DUSTT code, to be 2 - 200 ms and 22 - 4 cm with increasing the dust radius from 0.1 to 100 μm, respectively. Experimental and simulation results showed very few probability of the penetration into the confined plasma as an impurity source. On the other hand, the maximum velocities near the sublimation (0.01-0.1 km/s) are smaller and the lifetimes are longer than the measurement. Further improvement of the dust transport modelling such as ablation processes and initial velocity will be necessary.

Distribution of the dust in the vacuum vessel was investigated after 12 year operation of the W-shaped divertor. The total dust weights at the plasma-exposed surface and the shadow areas are estimated to be 1.32 g and 22.23 g, respectively. Microscope analysis showed that main population of small dust (less than 20 μm) has a statistical distribution, and that large dust (larger than 20 μm) was significant cumulated particularly on the exhaust route of gas flow under the divertor, which contributes mostly to the total weight. On the other hand, both the population of the small dust and number density of the large dust are necessary to evaluate the cumulative surface area, which will determines the tritium retention in dust.

References
[1] W. P. West, et al., Plasma Phys. Control. Fusion **48** (2006) 1661.
[2] D.L. Rudakov, et al., Nucl. Fusion, **49** (2009) 085022.
[3] K. Koga, et al., Plasma Fusion Res. **4** (2009) 034.
[4] N. Asakura, et al., Sec. 10.9 in JAEA-Review **2008-045** (2009) 161.
[5] T. Hatae, et al., Rev. Sci. Instrum. **70**, 772 (1999).
[6] A. Yu. Pigarov, et al., Phys. Plasmas **12** (2005) 122508.
[7] K. Masaki et al., J. Nucl. Mater. **337-339**(2005) 553.
[8] Y. Gotoh, et al., J. Nucl. Mater. **357** (2006) 138.
[9] N. Asakura, et al., Nucl. Fusion, **44** (2004) 503.
[10] S. I. Krasheninnikov, et al., Plasma Phys. Control. Fusion **50** (2008) 124054.
[11] Y. Tanaka, et al., submitted to J. Nucl. Mater.
[12] J. P. Sharpe, et al., J. Nucl. Mater. **337–339** (2005) 1000.